Toward Torque Control of a KUKA LBR IIWA for Physical Human-Robot Interaction

Vinay Chawda and Günter Niemeyer

***Abstract*— In this paper we examine joint torque tracking as well as estimation of external torques for the KUKA Lightweight Robot (LBR) IIWA. To support physical human-robot interaction tasks, we need smooth estimation that allows detection of delicate external events and good control to hide inertial forces. Unfortunately a transmission nonlinearity in the motor to joint gearing injects vibrations and limits the performance of the built-in torque controller and observer. We confirm the nonlinearity to be a spatially periodic deflection between the motor and joint. Identification of this behavior allows us to generate more accurate joint position measurements. We also design a matching spatial filter to remove the vibrations from joint torque measurements. Experiments on an LBR IIWA show that compensating for the nonlinearity provides smoother external torque estimates and improves the torque tracking performance. Furthermore, we are able to increase the gain margin more than three fold over the built-in controller.**

I. Introduction

The KUKA LBR IIWA, as seen in Fig. 1, is an industrial seven degree of freedom (DOF) serial manipulator intended for human-robot collaboration. It provides a suite of safety features that have allowed its certification to operate in human proximity [1], [2]. It also utilizes series elastic elements and benefits from a rich history of torque control and estimation reaching back to work at the German Aerospace Center DLR [3]. We are integrating the LBR into physical human-robot interaction tasks, which require accurate, stable and smooth control of joint torque and high sensitivity in detection of externally applied torques.

The LBR incorporates joint torque sensing, which it uses to control the internal and estimate any external torques. Close examination shows that the LBR has a nonlinearity in the motor to joint gearing which negatively impacts the performance of the torque control and observer. For example, in Fig. 2 we see external torque estimates obtained while the LBR moved without contact. At high speed the transmission nonlinearity causes vibrations, which the algorithm interprets as external torques.

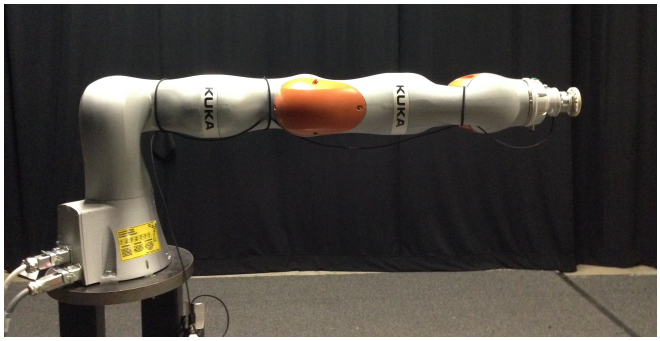

Fig. 1. The KUKA LBR IIWA with an ATI 6-axis Mini45 F/T sensor attached to the end-effector for measuring external torques. All data is given for the base joint, with the links arranged for maximum inertia as shown.

The authors are with Disney Research, Glendale, CA 91201, USA. Email: vinay.chawda@gmail.com, gunter.niemeyer@disneyresearch.com

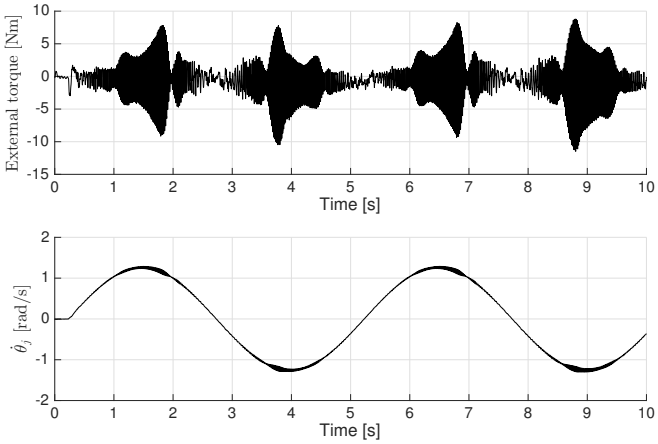

Fig. 2. External torque as reported by the FRI when sinusoidal torque profile was commanded to the built-in torque controller and no external torque was applied. It can be seen that the reported external torque estimates show large velocity dependent fluctuations and the velocities themselves show significant vibrations.

Fortunately, KUKA provides a Fast Robot Interface (FRI) that allows implementing external controllers at up to 1kHz loop rates. In this work we analyze the transmission nonlinearity and design adjustments to the measurements, controller, and estimation accordingly. In particular, we find a position dependent, spatially periodic deflection between the motor and joint angles, consistent with an eccentric motor to joint relationship. This allows us to compute an improved joint position estimate.

We also design a spatial filter to mitigate the fluctuations in the torque signals. Experiments conducted on an LBR IIWA show that leveraging the series elastic model, correcting for the transmission nonlinearity using a lookup table, and spatial filtering significantly improve the external torque estimates. Finally we create an additive controller using the spatially filtered joint torque for feedback, which improves the torque tracking performance and triples the gain margin.

II. LBR IIWA Review and Modeling

A. LBR IIWA Review

The KUKA LBR IIWA is a serial robotic arm with seven DOF and each joint is driven via a series elastic element con-

necting the motor and harmonic gear reducer to rigid links. Both motor position and joint or series elastic torques are sensed [1]. Additionally, a built-in external torque observer gives gravity canceled estimates of externally applied torques for each joint. KUKA provides a Fast Robot Interface (FRI) which allows real-time control of the LBR at up to 1kHz control loop rates [4]. The FRI can be switched between position or torque control modes, accepting commands for motor position or joint torque respectively. The torque commands are passed through a feasibility filter which imposes a maximum slew rate and torque control is suppressed when starting from zero velocity at torque levels below 1Nm.

Many torque control schemes have been proposed for physical human-robot interaction using the LBR or similar compliant manipulators ([5], [6], [7]). Geravand et al. similarly pursued physical human-robot interaction with a KUKA KR5 industrial manipulator using a closed control architecture [8]. In addition, previous works on LBR IIWA and it's predecessor LWR 4+ have reported full rigid body link dynamics [9], [10]. In the following, we focus on the low level motor motions and the associated nonlinearity that are the source of the problematic vibrations. As such, we isolate a single joint and present all data for the base joint with the other links arranged as shown in Fig. 1.

B. Joint Model

Using a lumped parameter model for a series elastic actuator ([11], [12]) and noting that motor friction and inertia are compensated by the internal torque controller [13], the system equations for a single joint with controlled inertia and damping can be written as:

$$J_c s^2 \theta_j = \frac{(b_c s + K)}{K}(\tau_c - \tau_J) \quad (1)$$

$$J_l s^2 \theta_l = \tau_J + \tau_{ext} \quad (2)$$

$$\tau_J = K(\theta_j - \theta_l) \quad (3)$$

where

J_l : Link inertia
J_c : Controlled motor inertia
b_c : Controlled motor friction
K : Series elastic stiffness
θ_j : Joint position
θ_l : Link position
τ_c : Commanded torque to the internal controller
τ_J : Series elastic joint torque
τ_{ext} : External torque

The FRI further adds a constant input delay of T_d = 5ms. The transfer function from τ_c to τ_J is given as:

$$\frac{\tau_J(s)}{\tau_c(s)} = e^{-T_d s} \frac{J_l(b_c s + K)}{J_c J_l s^2 + J_l b_c s + (J_c K + J_l K)} \quad (4)$$

We performed a frequency domain system identification using an exponential chirp excitation signal to estimate the transfer function parameters [14]. Fig. 3 shows the transfer function fit to the experimental frequency response. The identified values of the parameters are listed in Table I.

TABLE I
IDENTIFIED TRANSFER FUNCTION PARAMETERS

J_c :	1.03 kgm^2
b_c :	55 Nms/rad
K :	18500 Nm/rad
J_l :	5.6 kgm^2

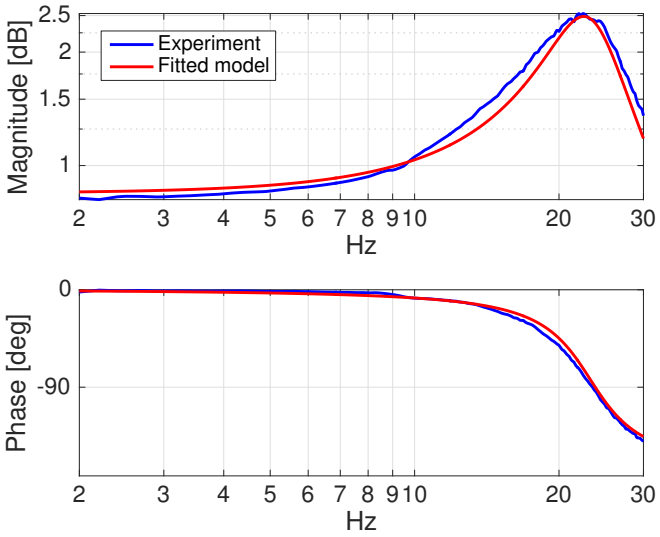

Fig. 3. Experimental frequency response and fitted transfer function response between commanded (τ_c) and measured joint torque (τ_J).

III. Transmission Nonlinearity

From Fig. 2 we have observed repeatable and velocity dependent joint vibrations. This is further illustrated in Fig. 4 where we see the vibration frequency correlate to joint velocity. The following experiments confirm a transmission nonlinearity in the LBR IIWA between the motor and joint, which causes fluctuations in their relative position.

A. Model

While the mechanical cause is unclear, the nonlinearity is consistent with eccentric gearing or a fluctuating gear reduction. We highly exaggerate this in the illustration in Fig. 5. The motor position maps to the joint position as

$$\theta_j = \theta_m - f(\theta_m \bmod \rho) \quad (5)$$

where the variation $f()$ repeats every $\rho = 0.01963$ rad.

B. Identification

We identified the nonlinearity both quasi-statically and dynamically. Statically, we commanded a constant torque and used a precision external measurement of the link position to deduce $\theta_j = \theta_l - \tau_J/K$. Fig. 6 graphs $\theta_m - \theta_j$ vs. θ_m under three commanded loads.

We further confirmed the data in dynamic tests. Moving the link at a high speed of $\dot{\theta}_l$=1.2 rad/s, the fluctuations occur at a frequency

$$f = \frac{\dot{\theta}_l}{\rho} = 61Hz \quad (6)$$

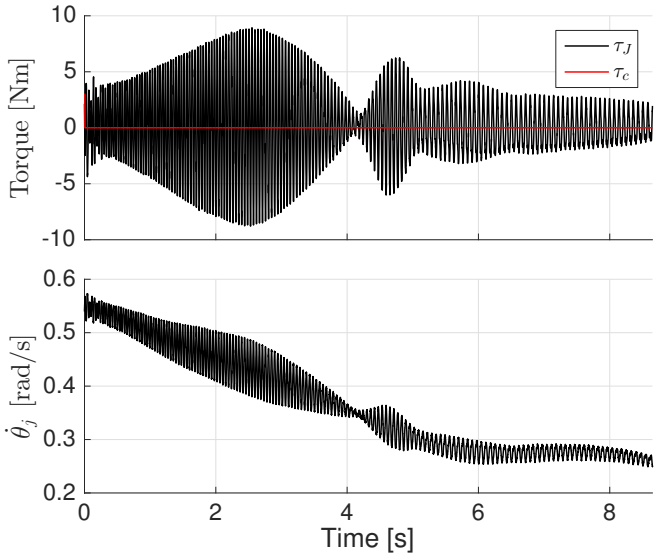

Fig. 4. Torque ripples change in frequency with velocity.

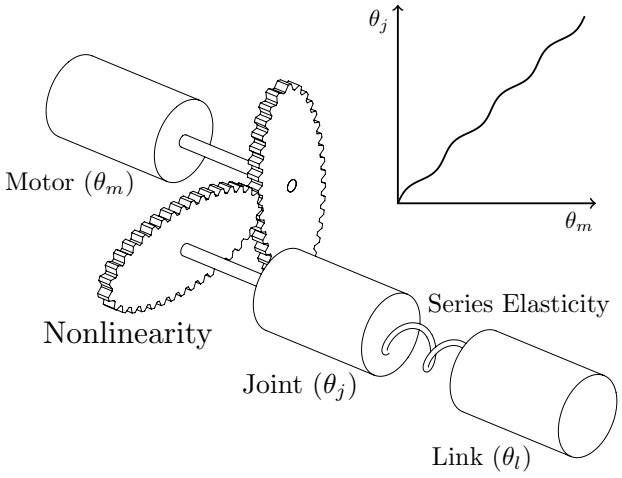

Fig. 5. A fluctuating gear reduction between the motor and joint could be the cause of the observed nonlinearity, which causes a periodic deflection between the joint and motor positions.

At this high frequency the series elastic stiffness K and link inertia J_l mostly block the fluctuations from affecting the link. The link fluctuations $\delta\theta_l$ can be estimated from the joint fluctuations $\delta\theta_j$ as

$$\delta\theta_l \approx \frac{K}{J_l(2\pi f)^2}\ \delta\theta_j = 0.0224\ \delta\theta_j \tag{7}$$

so that less than 2.3% of the fluctuations reach the link. In essence, we can assume the large link inertia holds the link velocity constant. This assumption then allows us establish θ_j independently of θ_m, using only joint torque measurements. The results are overlaid on Fig. 6. We see the periodic nature of the transmission nonlinearity holds true and matches well in both cases.

We note that the experimentally identified period $\rho = 0.01963$ rad also matches 327680 encoder ticks, where each

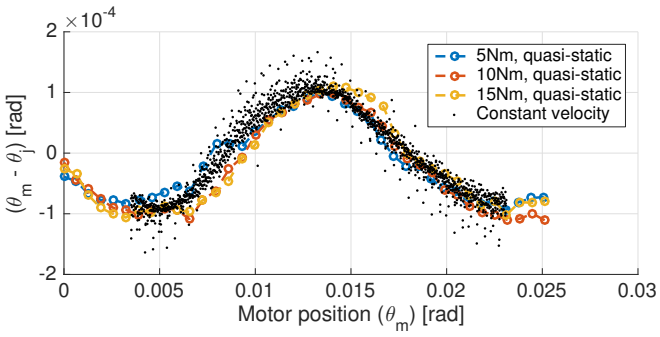

Fig. 6. Plots show variation of $\theta_m - \theta_j$ w.r.t. θ_m for quasi-static linear link motion against a constant commanded torque, and constant velocity motion under no external torque. Note that constant velocity data is wrapped around by plotting against (θ_m mod ρ) and shifted to match the phase with quasi-static data. Difference between motor (θ_m) and joint position (θ_j) is observed to be periodic with motor position. The period ρ was determined to be 0.01963 rad.

encoder tick is determined by the quantization of the sensor, which was determined to be 5.989×10^{-8} rad.

C. Position Measurement Adjustment

The transmission nonlinearity affects the joint and link, with their positions determined from the motor position and joint torque measurements as

$$\theta_j = \theta_m - f(\theta_m \bmod \rho) \tag{8}$$

$$\theta_l = \theta_m - f(\theta_m \bmod \rho) - \frac{1}{K}\tau_J \tag{9}$$

where we implement $f(\theta_m \bmod \rho)$ as a lookup table fitted to the experimental data.

D. Spatial Torque Filtering

Of course, the position fluctuation also impacts the joint torque. Though the exact magnitude and phase of any torque ripples depends on relative motor and joint inertia and friction, the frequency is directly proportional to speed. In Fig. 4 we see the vibrations slow exactly as the velocity slows.

We use knowledge of fixed spatial frequency to filter out torque variations due to the position fluctuations. First we define the spatial bandpass filter to isolate the fluctuations:

$$H_{ripple}(p) = \frac{\beta\omega p}{p^2 + \beta\omega p + \omega^2} \tag{10}$$

where p is the spatial Laplace transform of $^d/_{dx}$. We then apply the filter twice to increase the rolloff before subtracting from the original signal

$$H_{filt} = 1 - (\gamma H_{ripple})^2 \tag{11}$$

We inject the parameter:

$$\gamma = \begin{cases} 1.0 & \text{if } |\dot{\theta}_j| \geq v_{min} \\ \dfrac{|\dot{\theta}_j|}{v_{min}} & \text{if } |\dot{\theta}_j| < v_{min} \end{cases} \tag{12}$$

to limit filtering at slow speeds.

To implement we need to discretize the spatial filter. By definition a uniform spatial sampling is not possible, so we implement non-uniform spatial but uniform temporal sampling. A discrete time implementation is:

$$\begin{aligned} H_{ripple}(z) &= \frac{N(z)}{D(z)}, \text{ where} \\ N(z) &= (2\beta\omega\Delta) - (2\beta\omega\Delta)z^{-2}, \\ D(z) &= (4+2\beta\omega\Delta+\omega^2\Delta^2) + (2\omega^2\Delta^2-8)z^{-1} \\ &\quad +(4-2\beta\omega\Delta+\omega^2\Delta^2)z^{-2}, \end{aligned}$$

where Δ is the absolute change in joint position at any given time, $\omega = 2\pi/\rho$ is the spatial frequency of the fluctuations, and the parameter β decides the sharpness of the filter chosen to be 5.0.

In essence, this spatial filter matches a temporal filter with varying notch frequency of $\omega_n = (2\pi/\rho)\dot{\theta}_j$. As such, at low velocity the filter interacts with the controller. We thus pick $v_{min} = 0.2$ rad/s, which limits filtering below the frequency of $(2\pi/\rho)v_{min} = 10$ Hz.

IV. External Torque Estimation

The external torque estimates provided by the FRI use a disturbance observer introduced in [3], which for the single DOF case can be written as:

$$\begin{aligned} \hat{\tau}_{ext}(t) &= K_I\left[p(t) - \int_0^t (\tau_J + \hat{\tau}_{ext})dt - p(0)\right] \qquad (13) \\ p(t) &= J_l\dot{\theta}_l, \;\; \hat{\tau}_{ext}(0) = 0 \end{aligned}$$

where $\hat{\tau}_{ext}(t)$ is the external torque estimate. The value of observer gain K_I was identified to be 25 rad/s. We note the built-in observer ignores the series elastic compliance and uses $\dot{\theta}_j$ in place of $\dot{\theta}_l$ in (13). We are thus able to inject two improvements. First we utilize (9) to obtain the most accurate link velocity estimate in (13). Second, to remove the torque fluctuations we filter the torque estimate $\hat{\tau}_{ext}$ with the above spatial filter.

$$\hat{\tau}_{ext,filt} = H_{filt}\hat{\tau}_{ext} \qquad (14)$$

Fig. 7 compares estimates from various observers against the externally measured torque from an ATI mini45 6-axis F/T sensor attached to the end-effector. The robot arm was moved by hand under zero commanded torque. Using link velocity instead of motor velocity as described in (9) improves the estimates over built-in observer. Filtering further improves the estimates.

V. Torque Control

As the transmission nonlinearity injects fluctuations into the torque measurements, it also limits the built-in torque controller. We thus design and tune an additive torque controller to help increase damping, provide better tracking, and ultimately increase gain margins. In the following, we compare the nominal built-in controller to the additive design using step and sine wave inputs. Also, we use an external torque sensor to close the loop around both torque controllers and show that the additive controller can give ∼3x higher gain margin as compared to the built-in controller.

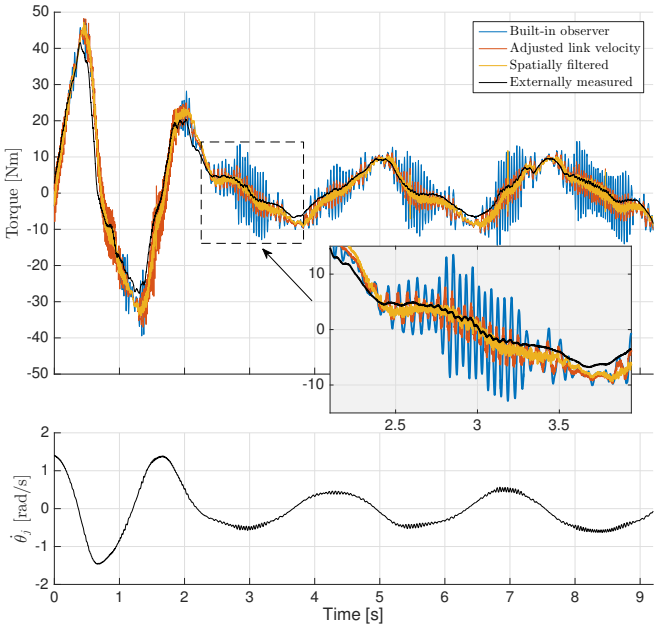

Fig. 7. Plots show external torque estimates from the built-in observer, the observer using adjusted link velocity ($\hat{\tau}_{ext}$), the spatially filtered estimate ($\hat{\tau}_{ext,filt}$), and an external torque measurement. The torque command τ_c was set to 0 and the robot arm moved externally by hand.

A. Built-in Torque Controller

In using the built-in controller, we set the commanded torque τ_c to a reference input τ_r. From the previous system identification, the poles are located at (-27.5 ± 143i, ω_n=23.24Hz, ζ=0.188). It can be seen from Fig. 8a that the response is underdamped with ∼ 40% overshoot. We also note that the natural frequency of 23Hz overlaps with the fluctuations if the arm is moving at a reasonable speed of 0.5 rad/s.

B. Additive Torque Controller

For the additive controller, we replace the delay in (4) with a 2nd order Padé approximation and design a full state observer and controller. The transfer function can be written as:

$$\frac{\tau_J(s)}{\tau_c(s)} = \left(\frac{s^2 - c_1 s + c_2}{s^2 + c_1 s + c_2}\right)\frac{J_l s^2(b_c s + K)}{J_c J_l s^4 + J_l b_c s^3 + (J_c K + J_l K)s^2}$$

where $c_1 = 1200$ and $c_2 = 480000$. The remaining parameters are specified in Table I. Using the spatial filter in (11), a filtered joint torque estimate $\tau_{J,filt}$ can be obtained:

$$\tau_{J,filt} = H_{filt}\tau_J \qquad (15)$$

A full state observer and controller can be expressed as

$$\tau_{fb} = -K_{FSF}\hat{X} + K_r\tau_r \qquad (16)$$

$$\dot{\hat{X}} = A\hat{X} + B\tau_{fb} + L(\tau_{J,filt} - C\hat{X}) \qquad (17)$$

$$\tau_c = \tau_{fb} + \tau_{ff} \qquad (18)$$

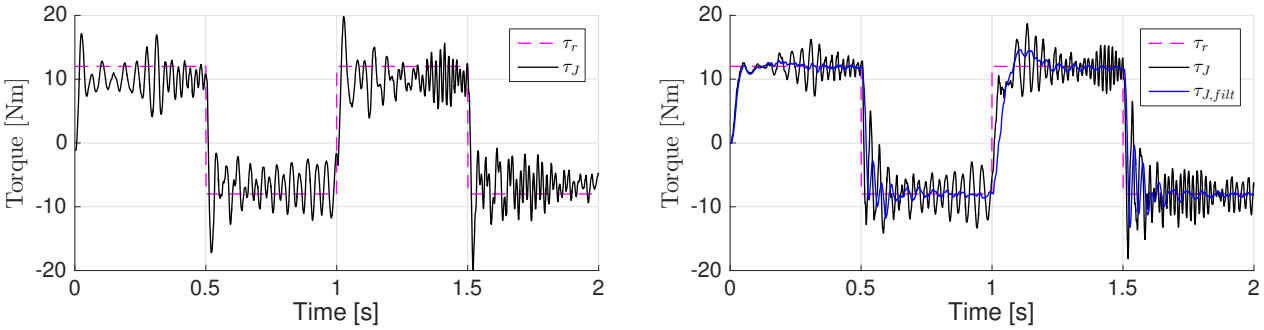

(a) Built-in torque controller

(b) Additive torque controller

Fig. 8. Step responses: We show the reference input, and joint torque in both controllers. The spatially filtered joint torque ($\tau_{J,filt}$) is also shown for the additive torque controller.

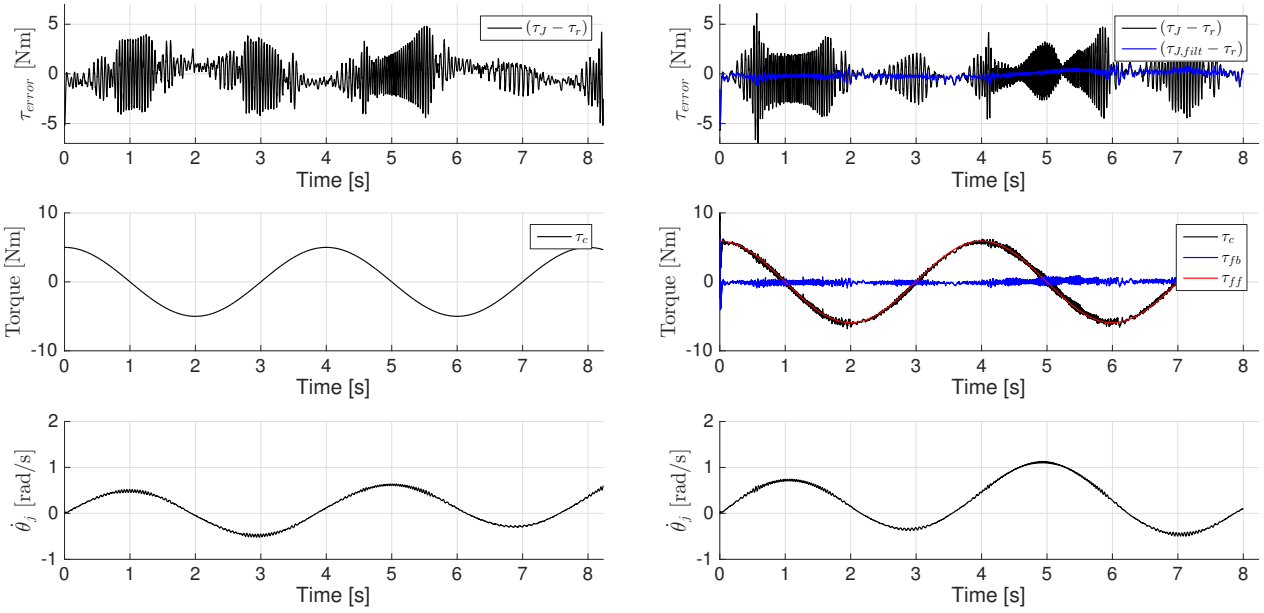

(a) Built-in torque controller, τ_r frequency = 0.25Hz

(b) Additive torque controller, τ_r frequency = 0.25Hz

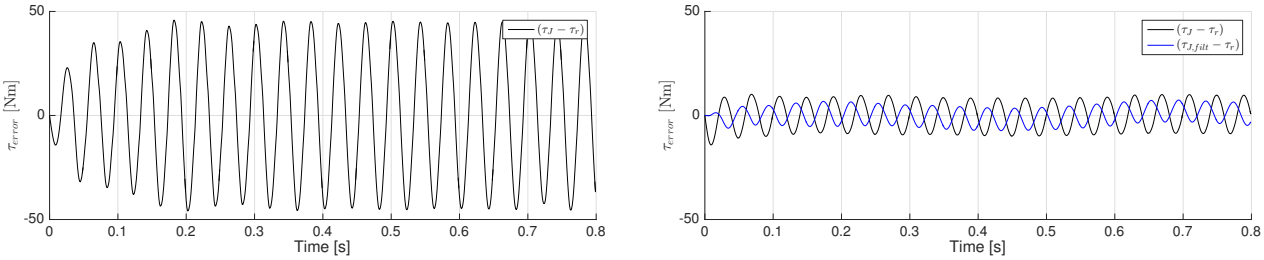

(c) Built-in torque controller, τ_r frequency = 25Hz

(d) Additive torque controller, τ_r frequency = 25Hz

Fig. 9. Sinusoidal reference torque waveform tracking with built-in controller and additive controller is shown for low (0.25Hz) and high (25Hz) frequency profiles. We see the built-in controller become unstable to a 25Hz input.

where

$$A = \begin{bmatrix} 0 & 0 & 0 & \left(-c_2K(\frac{1}{J_l}+\frac{1}{J_c})\right) \\ 1 & 0 & 0 & \left(-c_1K(\frac{1}{J_l}+\frac{1}{J_c})-c_2\frac{b_c}{J_c}\right) \\ 0 & 1 & 0 & \left(-K(\frac{1}{J_l}+\frac{1}{J_c})-c_1\frac{b_c}{J_c}-c_2\right) \\ 0 & 0 & 1 & \left(-\frac{b_c}{J_c}-c_1\right) \end{bmatrix}, \quad (19)$$

$$B = \begin{bmatrix} c_2\frac{K}{J_c} & (c_2\frac{b_c}{J_c}-c_1\frac{K}{J_c}) & (\frac{K}{J_c}-c_1\frac{b_c}{J_c}) & \frac{b_c}{J_c} \end{bmatrix}^T, \quad (20)$$

$$C = \begin{bmatrix} 0 & 0 & 0 & 1 \end{bmatrix} \quad (21)$$

and

$$\tau_{ff}(s) = \tau_r(s)\frac{J_cJ_ls^2 + J_lb_cs + (J_cK + J_lK)}{J_l(b_cs+K)} \quad (22)$$

The poles of the full state feedback controller are placed at (-180 $\pm$ 30i, ω_n=28.96Hz, ζ=0.986) and (-500 $\pm$ 1i, ω_n=79.58Hz, ζ=1.0). Observer poles are placed at (-620, ω_n=98.68Hz, ζ=1), (-630, ω_n=100.27Hz, ζ=1), (-1000, ω_n=159.16Hz, ζ=1) and (-1010, ω_n=95.65Hz, ζ=1). This gives the controller gains as:

$$K_{FSF} = \text{diag}(2.298\times10^{-8}\text{s}^3, -4.367\times10^{-6}\text{s}^2, 1.339\times10^{-3}\text{s}^1, -0.1516)$$
$$L = [3.843\times10^{11}\text{s}^{-4}, 1.996\times10^{9}\text{s}^{-3}, 3.346\times10^{6}\text{s}^{-2}, 2.005\times10^{3}\text{s}^{-1}]^T$$
$$K_r = 0.9636.$$

Since the controller is designed around the built-in controller, it is an additive torque controller.

The step responses in Fig. 8b shows a slight increase in damping, with some overshoot resulting from the nonlinear spatial filter.

C. Torque Tracking Performance

Sinusoidal reference torque profiles of $A = 5Nm$ at $f = 0.25Hz$ and $A = 15Nm$ at $f = 25Hz$ were used to test the tracking performance of the both controllers. Figs. 9a and 9b show the response for the $f = 0.25Hz$ profile. We see that while the unavoidable spatial fluctuations cause similar peak-to-peak errors for both controllers, the additive torque control scheme centers the mean error about zero.

Figs. 9c and 9d show the response for the $f = 25Hz$ profile. Here the built-in controller displays growing oscillations and settles with a large tracking error. Clearly the input, natural frequency, and fluctuations are interacting poorly. The additive torque controller however is still able to track with $\tau_{J,filt}$ tracking error < 5 Nm and τ_J tracking error < 10 Nm.

Finally, we attached an external force/torque sensor to the end-effector and used a direct $\tau_r = \kappa\tau_{ext}$ controller to reduce residual friction and inertial torques. The built-in controller started showing instabilities at a gain of $\kappa = 4.6$. Fortunately the additive controller remained stable through $\kappa = 15$. This more than triples the gain margin and means an external torque controller could hide three times the inertia in a physical interaction.

VI. Conclusion

In this paper we examined joint torque tracking for the KUKA LBR IIWA for physical human-robot interaction tasks. We found a transmission nonlinearity that creates substantial fluctuations and vibrations in both position and torque measurements. Fortunately the nonlinearity is spatially periodic and a simple lookup table can adjust/fix the position measurements. We were also able to design a spatial filter to remove vibrations from any torque signals.

Together, we were able to recover a smooth external torque observer and design an additive torque controller to improve performance and three fold increase gain margins.

We are finding the increased sensitivity invaluable in creating effective physical human-robot interactions and hope others may similarly leverage the benefits.

References

[1] KUKA Robotics. [Online]. Available: http://www.kuka-lbr-iiwa.com

[2] S. Shepherd and A. Buchstab, "Kuka robots on-site," in *Robotic Fabrication in Architecture, Art and Design*. Springer, 2014, pp. 373–380.

[3] A. D. Luca, A. Albu-Schaffer, S. Haddadin, and G. Hirzinger, "Collision detection and safe reaction with the dlr-iii lightweight manipulator arm," in *IEEE/RSJ International Conference on Intelligent Robots and Systems*, Oct 2006, pp. 1623–1630.

[4] "Kuka sunrise.connectivity fri 1.5 v3 manual," KUKA Roboter GmbH.

[5] S. Haddadin and E. Croft, *Physical Human–Robot Interaction*. Springer International Publishing, 2016, pp. 1835–1874.

[6] A. De Santis, B. Siciliano, A. De Luca, and A. Bicchi, "An atlas of physical human–robot interaction," *Mechanism and Machine Theory*, vol. 43, no. 3, pp. 253–270, 2008.

[7] R. Alami, A. Albu-Schaffer, A. Bicchi, R. Bischoff, R. Chatila, A. De Luca, A. De Santis, G. Giralt, J. Guiochet, and G. Hirzinger, "Safe and dependable physical human-robot interaction in anthropic domains: State of the art and challenges," in *IEEE/RSJ International Conference on Intelligent Robots and Systems*. IEEE, 2006, pp. 1–16.

[8] M. Geravand, F. Flacco, and A. De Luca, "Human-robot physical interaction and collaboration using an industrial robot with a closed control architecture," in *IEEE International Conference on Robotics and Automation (ICRA)*. IEEE, 2013, pp. 4000–4007.

[9] A. Jubien, M. Gautier, and A. Janot, "Dynamic identification of the kuka lightweight robot: Comparison between actual and confidential kuka's parameters," in *IEEE/ASME International Conference on Advanced Intelligent Mechatronics*, 2014, pp. 483–488.

[10] C. Gaz, F. Flacco, and A. De Luca, "Identifying the dynamic model used by the kuka lwr: A reverse engineering approach," in *International Conference on Robotics and Automation (ICRA)*. IEEE, 2014, pp. 1386–1392.

[11] A. Albu-Schäffer, C. Ott, and G. Hirzinger, "A unified passivity-based control framework for position, torque and impedance control of flexible joint robots," *The International Journal of Robotics Research*, vol. 26, no. 1, pp. 23–39, 2007.

[12] D. W. Robinson, J. E. Pratt, D. J. Paluska, and G. A. Pratt, "Series elastic actuator development for a biomimetic walking robot," in *IEEE/ASME International Conference on Advanced Intelligent Mechatronics*. IEEE, 1999, pp. 561–568.

[13] L. Le Tien, A. Albu-Schaffer, A. De Luca, and G. Hirzinger, "Friction observer and compensation for control of robots with joint torque measurement," in *IEEE/RSJ International Conference on Intelligent Robots and Systems*. IEEE, 2008, pp. 3789–3795.

[14] V. Chawda and G. Niemeyer, "Toward controlling a kuka lbr iiwa for interactive tracking," in *IEEE International Conference on Robotics and Automation (ICRA)*. IEEE, 2017.